

A GAIA SURVEY FOR YOUNG STARS ASSOCIATED WITH THE LUPUS CLOUDS¹K. L. LUHMAN^{2,3}*Draft version March 17, 2024*

ABSTRACT

I have used high-precision photometry and astrometry from the second data release of the Gaia mission to perform a survey for young stars associated with the Lupus clouds, which have distances of ~ 160 pc and reside within the Sco-Cen OB association. The Gaia data have made it possible to distinguish Lupus members from most of the stars in other groups in Sco-Cen that overlap with the Lupus clouds, which have contaminated previous surveys. The new catalog of candidate Lupus members should be complete for spectral types earlier than M7 at $A_K < 0.2$ within fields encompassing clouds 1–4. I have used that catalog to characterize various aspects of the Lupus stellar population. For instance, the sequence of low-mass stars in Lupus is ~ 0.4 mag brighter than the sequence for Upper Sco, which implies an age of ~ 6 Myr based on an adopted age of 10–12 Myr for Upper Sco and the change in luminosity with age predicted by evolutionary models. I also find that the initial mass function in Lupus is similar to that in other nearby star-forming regions based on a comparison of their distributions of spectral types.

1. INTRODUCTION

With distances of ~ 160 pc (Lombardi et al. 2008; Dzib et al. 2018; Zucker et al. 2020), the Lupus dark clouds are among the nearest sites of ongoing star formation (Comerón 2008). Because of their proximity, the stars born in those clouds are valuable for studies of the formation of stars and planets. Candidates for stars associated with the Lupus clouds have been identified via signatures of youth in the form of H α emission (Schwartz 1977), X-ray emission (Krautter et al. 1997), and mid- and far-infrared (IR) excesses (Allers et al. 2006; Allen et al. 2007; Chapman et al. 2007; Merín et al. 2008; Benedettini et al. 2018; Teixeira et al. 2020) and via optical and near-IR color-magnitude diagrams (CMDs, López Martí et al. 2005; Comerón et al. 2009; Comerón 2011; Mužić et al. 2014). Many of those candidates have been observed with spectroscopy to measure their spectral types and to help confirm their membership in the Lupus population with spectral signatures of youth (Appenzeller et al. 1983; Hughes et al. 1994; Krautter et al. 1997; Wichmann et al. 1999; Comerón et al. 2003, 2013; Torres et al. 2006; Allen et al. 2007; Mortier et al. 2011; Mužić et al. 2014, 2015; Alcalá et al. 2014, 2017; Frasca et al. 2017). The resulting samples of young stars can contain both members of Lupus and members of other populations in the Scorpius-Centaurus OB association (Sco-Cen, Preibisch & Mamajek 2008) that overlap on the sky with the Lupus clouds.

The Gaia mission (Perryman et al. 2001; de Bruijne 2012; Gaia Collaboration et al. 2016) has provided an all-sky catalog of precise parallaxes and proper motions that can reliably separate the stellar populations in

Sco-Cen. The second data release of Gaia (DR2) offers measurements of those parameters for stars down to $G \sim 20$ (Gaia Collaboration et al. 2018), which corresponds to substellar masses for unobscured members of Sco-Cen. Several studies have used the first two data releases of Gaia to identify candidate members of Lupus (Manara et al. 2018; Melton 2020; Teixeira et al. 2020) as well as Upper Scorpius, Ophiuchus, Upper Centaurus-Lupus (UCL), Lower Centaurus-Crux (LCC), and the V1062 Sco moving group (Cook et al. 2017; Goldman et al. 2018; Luhman et al. 2018; Röser et al. 2018; Wilkinson et al. 2018; Cánovas et al. 2019; Damiani et al. 2019; Esplin & Luhman 2020; Luhman & Esplin 2020). In this paper, I present a survey for members of Lupus using Gaia DR2 that improves upon previous work in terms of reducing contamination from the other associations in Sco-Cen (Section 2). I have used the resulting catalog of candidate members to characterize the age, disk fraction, initial mass function (IMF), and space velocities of the stellar population of Lupus clouds 1–4 and to constrain the presence of star formation in clouds 5 and 6 (Section 3).

2. IDENTIFICATION OF CANDIDATE MEMBERS OF LUPUS

2.1. *Defining Kinematic Membership Criteria*

The data products from Gaia DR2 employed in this study include photometry in bands at 3300–10500 Å (G), 3300–6800 Å (G_{BP}), and 6300–10500 Å (G_{RP}), proper motions and parallaxes ($G \lesssim 20$), and radial velocities ($G \sim 4$ –12). In addition, I have made use of the renormalized unit weight error (RUWE) from Lindegren (2018), which serves as an indicator of the goodness of fit for the astrometry. As done in Upper Sco by Luhman & Esplin (2020), I have adopted a threshold of $\text{RUWE} < 1.6$ when selecting astrometry that is likely to be reliable.

Because of projection effects, stars with similar space velocities (e.g., members of a young association) can exhibit a broad range of proper motions if they are dis-

¹ Based on observations made with the Gaia mission, the Two Micron All Sky Survey, the Wide-field Infrared Survey Explorer, the Spitzer Space Telescope, and the Visible and Infrared Survey Telescope for Astronomy Hemisphere Survey.

² Department of Astronomy and Astrophysics, The Pennsylvania State University, University Park, PA 16802; kll207@psu.edu.

³ Center for Exoplanets and Habitable Worlds, The Pennsylvania State University, University Park, PA 16802, USA

tributed across a large area of sky. As a result, populations with different space velocities can have overlapping proper motions. To reduce such projection effects and better distinguish the members of an association from other populations, one can analyze proper motions in terms of their offsets from the motions expected at the celestial coordinates and parallaxes of the stars for a characteristic space velocity for the association (e.g., the median velocity). These proper motion offsets have been utilized in recent studies of Gaia data in the Taurus star-forming region and populations in Sco-Cen (Esplin & Luhman 2017, 2019, 2020; Luhman 2018; Luhman & Esplin 2020) and are used in this work as well.

For my survey of Lupus, I have considered the area from $l = 335\text{--}345^\circ$ and $b = 5\text{--}19^\circ$, which is large enough to encompass clouds 1–6. A few additional small clouds are located near or just beyond the boundary of that field, but they do not show evidence of star formation (Comerón 2008). A map of extinction for the survey field is displayed in Figure 1 (Juvela & Montillaud 2016). For reference, I have marked the boundary between Upper Sco and UCL from de Zeeuw et al. (1999) and the fields that were mapped at $3.6\text{--}8\ \mu\text{m}$ by the Infrared Array Camera (IRAC; Fazio et al. 2004) on the Spitzer Space Telescope (Werner et al. 2004) during the facility’s cryogenic phase (Evans et al. 2003; Allers et al. 2006; Allen et al. 2007; Merín et al. 2008; Spezzi et al. 2011). The map does not include the IRAC observations of small areas ($\sim 5'$) toward individual stars between the Lupus clouds or the IRAC maps of the clouds performed during the post-cryogenic phase. The Multi-band Imaging Photometer for *Spitzer* (MIPS; Rieke et al. 2004) obtained images at $24\ \mu\text{m}$ for fields somewhat larger than the IRAC maps in Figure 1 (Chapman et al. 2007; Merín et al. 2008).

To characterize the kinematics of the dominant populations in Sco-Cen, Luhman & Esplin (2020) used data from Gaia DR2 to construct a diagram of $M_{G_{\text{RP}}}$ versus $G_{\text{BP}} - G_{\text{RP}}$ for the entire complex, selected candidate low-mass stars based on positions above the single-star sequence for the Tuc-Hor association (45 Myr, Bell et al. 2015), and identified clusters in the parallaxes and proper motion offsets of the resulting candidates. That analysis was applied to stars with $\pi > 5\ \text{mas}$, $\pi/\sigma \geq 20$, $\text{RUWE} < 1.6$, and $G_{\text{BP}} - G_{\text{RP}} = 1.4\text{--}3.4$ ($\sim \text{K5--M5}$, $\sim 0.15\text{--}1\ M_\odot$). I follow the same approach for determining the kinematics of stars associated with the Lupus clouds, except only the subsection of Sco-Cen selected for this survey is considered (Figure 1). In the top panel of Figure 2, I have plotted proper motion offsets versus parallax for the candidate young low-mass stars within that field. As done in Luhman & Esplin (2020), the proper motion offsets are computed relative to the motions expected for a space velocity of $U, V, W = -5, -16, -7\ \text{km s}^{-1}$, which approximates the median velocity of Upper Sco. That velocity is also similar to the median value for members of Lupus (Section 3.5). Three concentrations of stars are evident in the proper motion offsets and parallaxes in Figure 2. The middle population in parallax contains stars grouped near Lupus clouds 1–4 in both celestial coordinates and parallax (Lombardi et al. 2008; Dzib et al. 2018; Zucker et al. 2020). It also coincides with the kinematics of Upper Sco and likely includes

members of that association, as discussed in Section 3.2. The other two populations correspond to the V1062 Sco group and UCL.

Luhman & Esplin (2020) estimated probabilities of membership in three Sco-Cen populations (V1062 Sco, Upper Sco/Ophiuchus/Lupus, UCL/LCC) and a field population by applying a Gaussian mixture model (GMM) to the proper motion offsets and parallaxes for candidate young low-mass stars across the entirety of Sco-Cen. I have performed the same modeling on the data in the top panel of Figure 2 for my survey field containing the Lupus clouds, which is done using the *mcclust* package in R (R Core Team 2013; Scrucca et al. 2016). The resulting membership assignments to three components corresponding to Lupus (and Upper Sco), V1062 Sco, and UCL are indicated by the colors of the points in the middle panel of Figure 2. The stars that are more likely to reside in the field component have been omitted. Most stars have high probabilities of membership in a single component. For instance, 87 of the 94 stars in the Lupus component have membership probabilities of $> 80\%$. The spatial distributions of the members of the three GMM components are shown on maps in Figure 1. Most members of the V1062 Sco component are concentrated near that star ($l \sim 343.6^\circ$, $b \sim 5.2^\circ$) while the UCL component is widely scattered across the survey field. A majority of the stars assigned to the Lupus component are grouped near clouds 1–4. These maps illustrate that young stars with the kinematics of V1062 Sco and UCL represent a potential source of contamination in surveys for Lupus members that are based only on evidence of youth.

As shown in Figure 1, the GMM component for Lupus contains stars grouped near clouds 1–4 and a smaller number of stars that are widely scattered across the survey field. In Section 3.2, I find that the latter are likely to be members of Upper Sco, so I have attempted to refine the characterization of the kinematics of Lupus members by considering only the stars near the clouds. To do that, I have defined circular boundaries that encompass the groups of stars near clouds 2–4 and an elliptical boundary that is large enough to contain cloud 1, which are marked in Figure 1. In this study, stars within and outside of those boundaries are referred to as “on cloud” and “off cloud”, respectively. The bottom panel of Figure 2 shows the proper motion offsets and parallaxes of the 61 on-cloud members of the GMM component for Lupus. The distributions of those parameters are tighter with the omission of the off-cloud stars. The kinematics of the stars near cloud 1 exhibit small offsets relative to the stars near clouds 2–4. Dzib et al. (2018) found a similar shift when comparing the average proper motions of young stars near the clouds. Among the 61 on-cloud stars, 52 have been observed previously with spectroscopy, all of which have evidence of ages young enough for membership in Sco-Cen ($\lesssim 20\ \text{Myr}$). In the next section, I will use the proper motion offsets and parallaxes of the 61 on-cloud stars from the GMM component to define criteria for a search for candidate members of Lupus.

2.2. Applying Kinematic Membership Criteria

I have searched for members of Lupus by selecting stars from Gaia DR2 that have positions between $l = 335\text{--}345^\circ$

and $b = 5\text{--}19^\circ$ (the boundaries of the maps in Figure 1), $\pi/\sigma \geq 10$, and parallaxes and proper motion offsets that overlap at 1σ with those of the 61 on-cloud stars from the GMM component for Lupus in the bottom panel of Figure 2. The resulting sample contains 206 stars. To further refine these candidates, I have plotted them on diagrams of $M_{G_{RP}}$ versus $G_{BP} - G_{RP}$ and $M_{G_{RP}}$ versus $G - G_{RP}$ in Figure 3, which includes a fit to the single-star sequence for the Tuc-Hor association (45 Myr, Bell et al. 2015). Data with errors greater than 0.1 mag have been excluded. Nineteen stars appear in the diagram with $G - G_{RP}$ but not in the diagram with $G_{BP} - G_{RP}$. I have rejected the candidates that are likely too old to be members of Lupus based on positions in those diagrams near or below the sequence for Tuc-Hor. Stars with circumstellar disks can appear unusually faint for their color in CMDs due to short-wavelength excess emission from accretion or scattered light from an occulting disk, so all candidates with mid-IR excess emission indicative of disks have been retained. A total of 28 candidates were rejected based on the CMDs. Seven of the 206 candidates do not appear in either of the CMDs because they lack photometry in G_{BP} and G_{RP} . Six of these stars are possible companions to brighter stars that appear to be young in CMDs and the remaining candidate exhibits evidence of youth in the form of mid-IR excess emission, so these seven candidates are retained. After rejection of 28 candidates, there remain 178 candidates for kinematic members of Lupus.

It is likely that a small number of Lupus members were not selected by my kinematic criteria due to poor astrometric fits or large errors. Some of these members can be identified if they are companions to members that satisfied the kinematic criteria. I searched Gaia DR2 for stars that are located within $10''$ of any of the 178 kinematic candidates, have positions on CMDs that are consistent with membership, and have parallaxes and proper motions within the range of values in Sco-Cen. Nine candidate members were found in that manner, some of which have large values of RUWE, indicating poor astrometric fits, or have large parallax errors ($\pi/\sigma < 10$). These candidates consist of RX J1529.7-3628A, RX J1609.9-3923B, RX J1539.7-3450B, and sources 5997033290348155392, 5997083524280365056, 5994795990331624704, 6018569458962613888, 6035794025846997120, and 6007849461103724672 from Gaia DR2.

As an additional check for Lupus members that were missed by the kinematic criteria due to erroneous astrometry, I selected stars from Gaia DR2 that have positions in the on-cloud fields, $\pi/\sigma \geq 10$, CMD ages that are consistent with membership, and kinematics that do not satisfy my criteria for Lupus membership. For the resulting stars that exhibited signatures of youth from previous spectroscopy, I inspected the available astrometry for evidence that the Gaia DR2 measurements might be unreliable. Four stars were identified through this process, consisting of Gaia DR2 6011522757643072384, HD 142527, and Sz 108A/B. The first star is a $16''$ candidate companion to GQ Lup (Alcalá et al. 2020) and may have a poor astrometric fit (RUWE=2.25). HD 142527 is a well-studied Herbig Ae/Be star (Waelkens et al. 1996) that has a low-mass stellar companion at a separation of $< 0''.1$ (Biller et al. 2012; Close et al. 2014). It failed

the kinematic criteria due to its proper motion in declination from DR2 (-24.460 ± 0.052 mas yr $^{-1}$), but it satisfies the criteria if the significantly different measurement from DR1 is adopted (-26.336 ± 0.065 mas yr $^{-1}$). Sz 108A and B are known young stars (Appenzeller et al. 1983; Hughes et al. 1994; Comerón et al. 2003) that appear to comprise a binary system given their small separation ($4''$) but that exhibit different parallaxes and proper motions from Gaia DR2 (e.g., 6.61 ± 0.05 mas vs. 5.92 ± 0.12 mas). The individual stars do not satisfy the membership criteria in both the parallax and proper motion offsets, but the average values for the pair are consistent with membership (i.e., the kinematics of the stars are on opposite sides of the Lupus criteria). I have included these four stars in the sample of candidates.

The 191 candidate members of Lupus from the preceding analysis are presented in Table 1. The catalog includes previous measurements of spectral types and radial velocities, astrometry and photometry from Gaia DR2, UVW space velocities computed from the radial velocities and Gaia astrometry (Section 3.5), near-IR photometry from the Point Source Catalog of the Two Micron All Sky Survey (2MASS, Skrutskie et al. 2006) and other sources, mid-IR photometry from the AllWISE Source Catalog of the Wide-field Infrared Survey Explorer (WISE, Wright et al. 2010), flags for the presence of mid-IR excess emission and disk classifications (Section 3.3), and a flag indicating whether the celestial coordinates are within the circular and elliptical boundaries toward clouds 1–4 in Figure 1 (i.e., on cloud). For each pair of Gaia sources that is unresolved in 2MASS or WISE, the data from the latter surveys have been assigned to the component that is brighter in the G band with the exception of Sz 108 A/B, where the dominant component varies among the WISE bands. Among the 191 candidates in Table 1, 121 are on cloud and 106 have been observed previously with spectroscopy, all of which show evidence of youth ($\lesssim 20$ Myr) from Li I, gravity-sensitive absorption lines, or IR excess emission.

In addition to the Lupus candidates with Gaia kinematics in Table 1, I have compiled candidates that lack parallaxes and proper motions from Gaia and that are located within the circular and elliptical boundaries toward clouds 1–4 in Figure 1. I have retrieved sources from the 2MASS Point Source Catalog within those fields and have rejected those that have Gaia kinematics or CMDs that are inconsistent with membership and those that are not young stars based on other available data (e.g., resolved galaxies). The number of remaining stars is low down to $H \sim 14$ and increases rapidly at fainter magnitudes. I have adopted the 18 unrejected 2MASS sources at $H < 14$ as candidates. Among those candidates, 10 have previous spectral classifications, 12 exhibit evidence of youth from spectroscopy or mid-IR excess emission, and 13 have counterparts in Gaia DR2. All of the latter stars have large values of RUWE that indicate poor astrometric fits, which explains the absence of accurate measurements of parallaxes and proper motions. I also have examined available constraints on membership for candidates for disk-bearing stars that have been previously identified in mid- and far-IR imaging (e.g., Merín et al. 2008; Benedettini et al. 2018) and that lack Gaia data. Five of those stars are adopted as candidate members, which include the known protostars

IRAS 15398–3359 and Lupus 3 MMS. The combined sample of 23 on-cloud candidates lacking Gaia kinematics is presented in Table 2, which contains the same data as in Table 1 with the exception of the kinematic data. The 0′7 companion GQ Lup B is an additional probable member of Lupus (Neuhäuser et al. 2005), but it is omitted from Table 2 because it lacks most of the tabulated measurements.

2.3. Comparison to Previous Surveys

Several previous studies have presented candidate members of Lupus. For the candidates with measurements of parallaxes and proper motions from Gaia, I have examined whether they appear in my catalog of candidates. If not, I have used the Gaia data to assess whether the candidates are field stars or members of other populations in Sco-Cen.

Krautter et al. (1997) identified young stars in a large area surrounding the Lupus clouds through optical spectroscopy of X-ray sources, 74 of which are located within the field considered in this work ($l = 335\text{--}345^\circ$, $b = 5\text{--}19^\circ$) and have parallaxes and proper motions from Gaia DR2. Based on the Gaia kinematics, I have classified 14 as candidate Lupus members, 17 as field stars, and 43 as candidate members of other populations in Sco-Cen (primarily UCL). It is not surprising that a wide-field survey for young stars would be dominated by the latter given the results in Figure 1.

Allen et al. (2007) selected 19 candidates for disk-bearing stars from Spitzer images of cloud 3, 10 of which were confirmed as young stars through spectroscopy in that work and subsequent studies (Mortier et al. 2011; Mužić et al. 2015; Alcalá et al. 2014, 2017). Based on Gaia parallaxes and proper motions, I have classified the confirmed young stars as six candidate members of Lupus, three candidate members of other Sco-Cen groups, and one field star, although the errors for two stars are fairly large ($\sim 15\%$ in parallax). Gaia data are available for two of the nine candidates from Allen et al. (2007) that lack spectra, which I classify as a background star and a candidate member of V1062 Sco or UCL. Four additional candidates that lack spectra are galaxies (Comerón 2011; Comerón et al. 2013, VISTA).

Merín et al. (2008) presented a large sample of candidate young stars from Spitzer images of clouds 1, 3, and 4. Among the 126 candidates with Gaia kinematics, I have classified 56 as Lupus candidates, 22 as candidate members of other groups in Sco-Cen, and 48 as unrelated to Sco-Cen. This level of contamination by other Sco-Cen groups is consistent with the surface densities of their kinematic members (Damiani et al. 2019, Figure 1).

Comerón et al. (2009) identified candidate members of Lupus using optical images of clouds 1, 3, and 4 that encompassed the Spitzer fields from Merín et al. (2008). Based on my kinematic analysis, the 140 stars with Gaia parallaxes and proper motions consist of 19 candidate Lupus members, 19 candidate members of the remainder of Sco-Cen, and 102 objects that are unrelated to Sco-Cen. Comerón et al. (2013) also found that many of the candidates are background stars based on spectroscopy.

Manara et al. (2018) used kinematic data from Gaia DR2 to examine the membership of candidate members of clouds 5 and 6 from Spezzi et al. (2011). They found that five candidates exhibit parallaxes and proper

motions that are suggestive of membership in Lupus while the remaining candidates with Gaia data are background stars. One of those five candidates satisfies my kinematic criteria for Lupus membership (Gaia DR2 6021805356032645504), one has a discrepant parallax for Lupus (Gaia DR2 6021745462701109376, $\pi = 8.91 \pm 0.19$ mas), and the remaining three candidates are just beyond my kinematic thresholds for selection for Lupus (Gaia DR2 6021420630046381440, 6021662385163162240, 6021662385163163648).

Damiani et al. (2019) used Gaia DR2 to identify candidate members of various populations in Sco-Cen, including cloud 3 in Lupus. For the 69 stars assigned to that cloud, I have classified 61 as Lupus candidates, five as candidate members of other Sco-Cen groups, and three as unrelated to Sco-Cen.

Melton (2020) assumed Lupus membership for 154 previously identified candidate members that had Gaia parallaxes and proper motions and searched Gaia DR2 for additional candidates that exhibited similar kinematics. I find that 65 of the stars adopted as members have kinematics inconsistent with membership in Lupus, most of which are likely members of other populations in Sco-Cen. Because the adopted Lupus members were contaminated by non-members, the candidates identified in that search of Gaia DR2 were contaminated as well. Among the 431 candidates, 50 are classified as Lupus candidates in this work while the remaining stars are classified as non-members.

Teixeira et al. (2020) selected candidate disk-bearing stars in a large field encompassing the Lupus clouds ($l = 330\text{--}349^\circ$, $b = 1.6\text{--}27.6^\circ$) using mid-IR photometry from WISE. They checked whether the candidates were likely to be members of Lupus, UCL, V1062 Sco, or Upper Sco by comparing their proper motions and parallaxes to those of previously proposed members. Lupus and UCL appeared to have indistinguishable proper motions, so candidates were classified as members of either of those two populations. However, I find that Lupus and UCL do exhibit distinct kinematics when analyzed in terms of proper motions that have been corrected for projection effects (Figure 2) and when the previous samples in Lupus members are vetted for contamination from UCL and other groups in Sco-Cen. Teixeira et al. (2020) presented 60 candidate members of Lupus or UCL, three of which are among my kinematic Lupus candidates in Table 1. I classify the remaining 57 candidates as field stars or members of other groups in Sco-Cen based on their parallaxes and proper motion offsets.

3. PROPERTIES OF THE LUPUS STELLAR POPULATION

3.1. Spectral Types and Extinctions

I seek to characterize the stellar population associated with the Lupus clouds in terms of its age, disk fraction, IMF, and space velocities using the candidate members from Tables 1 and Table 2. Some of this analysis requires estimates of extinctions and spectral types. For stars with previously measured spectral types, I have estimated extinctions from color excesses in $G_{\text{RP}} - J$ or $J - H$ (in order of preference) relative to the typical intrinsic colors of young stars from Luhman & Esplin (2020). The reddenings are converted to extinctions in K_s using relations from Indebetouw et al. (2005) and Schlafly et al.

(2016) and $E(G_{\text{RP}} - J)/E(J - H) \approx 2.4$, where the latter is based on reddened members of Upper Sco and Ophiuchus (Esplin & Luhman 2020; Luhman & Esplin 2020).

For stars that lack spectral classifications, I have estimated spectral types and extinctions by dereddening their observed colors to the sequence of intrinsic colors of young stars in diagrams of $G_{\text{RP}} - J$ versus $J - H$ or $J - H$ versus $H - K_s$, which are shown in Figure 4 for the Lupus candidates. Since the sequence of intrinsic colors in $G_{\text{RP}} - J$ versus $J - H$ is largely parallel to the reddening vector at earlier types, spectral types and extinctions are estimated from that diagram only for $G_{\text{RP}} - J > 1.3$ (M types). With the exception of a few stars with $J - H$ excesses from disks, the stars at $G_{\text{RP}} - J < 1.3$ are quite close to the sequence of intrinsic colors, so they are assumed to have no extinction and their spectral types are estimated from the observed values of $G_{\text{RP}} - J$. For the few stars that lack G_{RP} but have JHK_s , spectral types and extinctions are estimated from $J - H$ versus $H - K_s$ if photometry at longer wavelengths does not show excess emission from circumstellar dust (Section 3.3). For companions that have only Gaia photometry, the extinctions of their primary stars are adopted, and their spectral types are estimated from extinction-corrected $G_{\text{BP}} - G_{\text{RP}}$ if available. If a companion only has G photometry, a spectral type is derived from the median relation between extinction-corrected G and spectral type among the candidates that have spectral classifications. I have not attempted to estimate spectral types and extinctions for the small number of candidates with $J - H > 1.2$ ($A_K \gtrsim 0.5$ for M stars) since the upcoming analysis that involves those parameters (Sections 3.2 and 3.4) excludes stars with high extinctions.

3.2. Stellar Ages

The age of a young stellar population can be constrained via its sequence of low-mass stars in the Hertzsprung-Russell (H-R) diagram. Photometry in a single band and either spectral types or colors can serve as substitutes for bolometric luminosities and effective temperatures, respectively. For instance, in a recent study of Ophiuchus, Esplin & Luhman (2020) analyzed ages using an IR photometric band and spectral types since optical photometry and colors would be significantly affected by the high extinction among many of the members of that region. For Lupus, most of the candidate members have only modest extinction (Figure 4) and many of them lack spectral classifications, so the high-precision optical photometry from Gaia is the best option for both axes of the H-R diagram (i.e., a CMD). The same approach was taken by Luhman & Esplin (2020) when comparing the ages of Upper Sco, UCL, LCC, and V1062 Sco, all of which have low extinction.

In the top row of Figure 5, I have plotted diagrams of $M_{G_{\text{RP}}}$ versus $G_{\text{BP}} - G_{\text{RP}}$ and $M_{G_{\text{RP}}}$ versus $G - G_{\text{RP}}$ for Lupus candidates from Table 1 that have $\pi/\sigma \geq 20$ and $A_K < 0.2$ and that lack full disks (Section 3.3). Stars with full disks have been omitted because G_{BP} is susceptible to accretion-related emission at short optical wavelengths. The photometry in the CMDs has been corrected for the extinctions estimated in the previous section. The on- and off-cloud candidates are plotted with different symbols in Figure 5, which shows that the off-cloud stars are systematically fainter at a given color,

indicating older ages. The off-cloud stars also exhibit a lower disk fraction (Section 3.3), which is consistent with older ages.

In the bottom row of Figure 5, the off-cloud candidates are compared to diskless members of Upper Sco that have $\pi/\sigma \geq 20$ and $A_K < 0.1$ (Luhman & Esplin 2020). The lower envelopes of the sequences for those two samples are roughly aligned in absolute magnitude, which suggests that the oldest off-cloud stars are coeval with Upper Sco (10–12 Myr, Pecaute et al. 2012; Pecaute & Mamajek 2016; Luhman & Esplin 2020). For the colors corresponding to K4–M5 ($G_{\text{BP}} - G_{\text{RP}} \sim 1.4$ – 3.3 , $G - G_{\text{RP}} \sim 0.7$ – 1.3), the sequences for the on-cloud Lupus candidates in the two CMDs are ~ 0.4 mag brighter than the sequences for Upper Sco. If the latter has an age of 10–12 Myr, that difference implies an age of 5.2–6.5 Myr for Lupus based on non-magnetic evolutionary models (Baraffe et al. 2015; Choi et al. 2016; Dotter 2016) and new versions of the magnetic models from Feiden (2016) provided by G. Feiden (private communication). The sample of on-cloud candidates in Figure 5 contains 30 stars near cloud 3 and only 1–9 stars near each of the other clouds, so the numbers of stars are too small for a comparison of ages among the clouds.

Given the difference in mean ages of the on- and off-cloud Lupus candidates, most of the off-cloud candidates are probably not associated with the Lupus clouds. Instead, they are likely members of a low-density, distributed component of Upper Sco that extends into the survey field (see the nominal boundary between Upper Sco and UCL in Fig. 1), which is supported by the coevality of the oldest off-cloud candidates with Upper Sco and the fact that the Lupus candidates have parallaxes and proper motion offsets within the ranges of values exhibited by Upper Sco (Luhman & Esplin 2020). Therefore, the best sample of Lupus candidates consists of the on-cloud stars in Table 1 and the candidates in Table 2 (all of which are on cloud). The surface density of off-cloud candidates implies that the on-cloud sample could contain ~ 10 stars that are members of Upper Sco rather than Lupus. Meanwhile, it is possible that a few of the off-cloud candidates are associated with the Lupus clouds.

3.3. Disk Fraction

I have used mid-IR photometry from WISE and the Spitzer Space Telescope to check for evidence of circumstellar disks around the candidate members of Lupus. WISE obtained images in bands centered at 3.5, 4.5, 12, and 22 μm , which are denoted as W1, W2, W3, and W4, respectively. Spitzer observed primarily in bands at 3.6, 4.5, 5.8, 8.0 and 24 μm , which are denoted as [3.6], [4.5], [5.8], [8.0], and [24], respectively. As mentioned in Section 2.1, Spitzer has imaged areas encompassing most of the Lupus clouds (Figure 1) as well as small fields toward individual stars between the clouds. As an all-sky survey, WISE provides images that cover all of the Lupus candidates, but it offers lower sensitivity and angular resolution than Spitzer.

As done in previous disk surveys by Luhman & Mamajek (2012) and Esplin et al. (2014, 2018), I have used the extinction-corrected colors between K_s and six bands from WISE and Spitzer (W2, W3, W4, [4.5], [8.0], [24]) to detect excess emission from disks. For each extinction-corrected color,

I have subtracted the typical intrinsic color for the spectral type in question (Luhman & Esplin 2020). The resulting color excesses are used to determine whether significant disk emission is present and to classify the evolutionary stages of any detected disks (Esplin et al. 2014, 2018). The adopted disk classes consist of the following (Kenyon & Bromley 2005; Rieke et al. 2005; Hernández et al. 2007; Luhman et al. 2010; Espaillat et al. 2012): full (optically thick with no large holes), transitional (optically thick with a large hole), evolved (optically thin with no large hole), evolved transitional (optically thin with a large hole), and debris disk (second generation dust from planetesimal collisions). For reference, young stars and their circumstellar material can be classified in the following manner (Lada & Wilking 1984; Lada 1987; André et al. 1993; Greene et al. 1994): classes 0 and I (protostar with an infalling envelope and a full disk), class II (star with a primordial disk but no envelope), and class III (star that no longer has a primordial disk but that can have a debris disk). The class II disks include full, transitional, evolved, and evolved transitional, although the latter are sometimes counted as class III when calculating disk fractions since they are indistinguishable from debris disks in mid-IR data.

The color excesses for the Lupus candidates are plotted in Figure 6. Tables 1 and 2 include flags that indicate whether excesses are detected in W2, W3, W4, [4.5], [8.0], and [24] and the classifications of the disks. A few of the Lupus candidates are listed in Tables 1 and 2 as class 0 or class I based on previous work. Candidates that do not show excesses in their mid-IR data are labeled as class III. Among the 214 candidates in Tables 1 and 2, 17 lack mid-IR photometry because they are below the detection limits of the available imaging or are unresolved from brighter companions.

Most of the disks identified in my analysis have been found in previous studies (Evans et al. 2003; Padgett et al. 2006; Cieza et al. 2007; Merín et al. 2008, 2010; Wahhaj et al. 2010; Romero et al. 2012; Bustamante et al. 2015; Pecaut & Mamajek 2016; Benedettini et al. 2018). The newly detected disks include three transitional disks (Sz 127, Gaia DR2 6013489268547136768, Gaia DR2 6035036466655228672) and two evolved disks (Gaia DR2 5995219680274444672, Gaia DR2 6014623517871055488). Sz 127 has been classified as M5 (Hughes et al. 1994) while the remaining four stars have not been observed with spectroscopy. Gaia DR2 6013489268547136768 and 6035036466655228672 are far from the Lupus clouds, so they are probably members of Upper Sco (Section 3.2).

As in Luhman et al. (2010), I have defined the disk fraction as the ratio of the number of class II objects to the number of stars in classes II and III. I also count evolved transitional disks as class III. Among the Lupus candidates in Tables 1 and 2 that have mid-IR data, the disk fraction is 82/131 (0.63 ± 0.04) for on-cloud stars and 13/62 ($0.21^{+0.06}_{-0.04}$) for off-cloud stars. The lower disk fraction for the off-cloud stars is consistent with the older ages that they exhibit in the CMDs (Section 3.2). The off-cloud stars are roughly coeval with members of Upper Sco in the CMDs, and their disk fractions are similar as well (Luhman & Esplin 2020), which supports the sug-

gestion from Section 3.2 that most of the off-cloud stars are members of Upper Sco. To further illustrate that the youngest candidates are concentrated near the Lupus clouds, I have plotted in Figure 7 one map with all candidates from Tables 1 and 2 and a second map with only the candidates with the least evolved disks (full disks).

3.4. Initial Mass Function

As done in my previous work on nearby star-forming regions (e.g., Luhman et al. 2016; Luhman & Esplin 2020), I have characterized the IMF in Lupus in terms of the distribution of spectral types, and I have constructed that distribution for an extinction-limited sample of candidate members. I have selected a limit of $A_K < 0.2$ for that sample, which is high enough to include a large majority of candidates while low enough that the sample is complete down to low masses. In Section 2.2, I found that my survey of Lupus should be complete down to $H \sim 14$ for the on-cloud fields, which corresponds to $\sim M7$ for $A_K = 0.2$. For candidates that lack spectral classifications, I have used spectral types estimated from photometry in the manner described in Section 3.1. The top diagram in Figure 8 shows the distribution of spectral types for on-cloud candidates from Tables 1 and 2 that have $A_K < 0.2$. For comparison, I have included distributions for samples of stars in Upper Sco (Luhman & Esplin 2020), Taurus (Esplin & Luhman 2019), and IC 348 (Luhman et al. 2016). The distributions for Lupus and those regions are similar, indicating similar IMFs.

3.5. Radial Velocities and UVW Velocities

Table 1 includes previous measurements of radial velocities that have errors less than 4 km s^{-1} , which are available for 78 Lupus candidates. I have adopted errors of 0.4 and 1 km s^{-1} for velocities from Torres et al. (2006) and Wichmann et al. (1999) for which errors were not reported, respectively, which are near the typical precisions estimated in those studies. For the 78 stars with radial velocities and Gaia measurements of proper motions and parallaxes, I have used the radial velocities, proper motions, and parallactic distances (Bailer-Jones et al. 2018) to compute UVW space velocities (Johnson & Soderblom 1987), which are listed in Table 1. Errors in the space velocities were estimated in the manner described by Luhman & Esplin (2020).

Table 3 lists the medians and standard deviations of the UVW velocities of candidates within the boundaries of clouds 1–4 from Figure 1. These parameters are provided for each cloud and for the combined sample of 69 stars from the four clouds. The median velocities vary by a few km s^{-1} among the Lupus clouds and they differ by a similar amount from the value of $(-5.1, -16.0, -7.2) \text{ km s}^{-1}$ for Upper Sco (Luhman & Esplin 2020). The radial velocity errors tend to be greater than the equivalent errors in proper motion, and the former contribute primarily to the errors in U , which is why the standard deviations are largest in that velocity component. The standard deviations of the velocities serve as upper limits on the velocity dispersions.

3.6. Constraints on Star Formation in Clouds 5 and 6

Clouds 1–4 have been previously known to harbor star formation based on the clustering of young stars near

them on the sky and the presence of significant reddening toward some of those stars (Comerón 2008, references therein). Clear evidence of star formation has been lacking for the remaining Lupus clouds. Two of those clouds, 5 and 6, are within the field selected for my survey (Figure 1). The best available constraints on star formation in clouds 5 and 6 have been provided by Spitzer images (Spezzi et al. 2011), which were capable of identifying disk-bearing stars at substellar masses and high extinctions. Spezzi et al. (2011) found 15 candidates for disk-bearing stars based on mid-IR excesses. Using parallaxes from Gaia DR2, Manara et al. (2018) classified eight candidates as background stars and four candidates as possible members of clouds 5 and 6. However, as mentioned in Section 2.3, I find that only one of the latter stars has kinematics consistent with Lupus membership. Given that the off-cloud Lupus candidates appear to be dominated by Upper Sco members (Section 3.2), that candidate is probably a member of Upper Sco as well. The three remaining disk-bearing candidates from Spezzi et al. (2011) lack Gaia parallaxes and confirmation of their youth. Thus, it is likely that clouds 5 and 6 have not have experienced star formation.

4. CONCLUSIONS

I have performed a survey for stars associated with the Lupus clouds using high-precision photometry and astrometry from Gaia DR2. The new catalog of candidate members has been used to characterize the age, disk fraction, IMF, and space velocities of the stellar population of clouds 1–4 and to constrain the presence of star formation in clouds 5 and 6. The results are summarized as follows:

1. For an area within Sco-Cen that encompasses most of the Lupus clouds ($l = 335\text{--}345^\circ$, $b = 5\text{--}19^\circ$), I have 1) identified candidate young low-mass stars based on their positions in CMDs, 2) fit their kinematics with a Gaussian mixture model that contains components for Lupus, the V1062 Sco group, and UCL, 3) defined kinematic criteria for membership in Lupus based on the stars in the Lupus component that are grouped near clouds 1–4, 4) searched Gaia DR2 for stars within the survey field that satisfy those criteria, and 5) rejected the Gaia sources that appear to be too old for membership in Sco-Cen based on CMDs. This process has produced 178 candidate members of Lupus. I also have attempted to identify Lupus members that have Gaia kinematics but that failed my criteria due to erroneous astrometry, resulting in 13 additional candidates. These 178 and 13 candidates with Gaia kinematics are presented in Table 1.
2. I have examined previous IR surveys for viable Lupus candidates near clouds 1–4 that lack measurements of kinematics from Gaia. The resulting sample of 23 candidates is provided in Table 2. The sample of candidates near clouds 1–4 from Tables 1 and 2 should be complete for spectral types earlier than M7 at $A_K < 0.2$.
3. Based on the kinematic data from Gaia, many of the young stars previously identified as possible

members of Lupus are instead members of other populations in Sco-Cen that overlap with the Lupus clouds (e.g., UCL).

4. According to CMDs and disk fractions, the Lupus candidates far from clouds 1–4 are older than the candidates near those clouds and are coeval with the Upper Sco association (10–12 Myr). Given that the off-cloud candidates (like all of the Lupus candidates) share similar kinematics with Upper Sco, they are probably members of a low-density, distributed component of Upper Sco that extends into the survey field. Thus, the 144 on-cloud candidates in Tables 1 and 2 represent the best available sample of stars associated with the Lupus clouds.
5. At spectral types of $\sim K4\text{--}M5$ in Gaia CMDs, the sequence of on-cloud Lupus candidates is ~ 0.4 mag brighter than the sequence for Upper Sco, which implies an age of ~ 6 Myr for Lupus assuming an age of 10–12 Myr for Upper Sco and the change in luminosity with age predicted by evolutionary models (Baraffe et al. 2015; Choi et al. 2016; Dotter 2016; Feiden 2016).
6. I have used mid-IR photometry from WISE and the Spitzer Space Telescope to check the Lupus candidates for excess emission from circumstellar disks and have classified the evolutionary stages of the detected disks. Most of the disks among these candidates have been reported in previous studies, but I point out a few examples of new disks in more advanced stages of evolution. The disk fraction for the on-cloud candidates is $N(\text{II})/N(\text{II}+\text{III})=0.63 \pm 0.04$.
7. Using spectroscopic and photometric estimates of spectral types, I have constructed a distribution of spectral types for an extinction-limited sample of on-cloud candidates. It is similar to the distributions in other nearby star-forming regions, indicating a similar IMF.
8. By combining Gaia parallaxes and proper motions with previous measurements of radial velocities, I have calculated UVW space velocities for 78 candidate members of Lupus, including 69 of the on-cloud candidates. The median space velocities of the groups near clouds 1–4 vary by a few km s^{-1} and differ by a similar amount from the median velocity of Upper Sco.
9. Previous Spitzer imaging has identified 15 candidate disk-bearing stars toward clouds 5 and 6 (Spezzi et al. 2011), eight of which are background stars based on Gaia parallaxes and three of which lack Gaia parallaxes (Manara et al. 2018). I find that the remaining four stars are probably members of other groups in Sco-Cen. Thus, I find no evidence of stars associated with clouds 5 and 6.

I thank Taran Esplin and Eric Mamajek for comments on the manuscript. This work used data

from the European Space Agency (ESA) mission Gaia (<https://www.cosmos.esa.int/gaia>), processed by the Gaia Data Processing and Analysis Consortium (DPAC, <https://www.cosmos.esa.int/web/gaia/dpac/consortium>). Funding for the DPAC has been provided by national institutions, in particular the institutions participating in the Gaia Multilateral Agreement. 2MASS is a joint project of the University of Massachusetts and IPAC at Caltech, funded by NASA and the NSF. WISE is a joint project of the University of California, Los Angeles, and the JPL/Caltech, funded by NASA. This work used data from the Spitzer Space Telescope and the NASA/IPAC Infrared Science Archive, operated by JPL under contract with NASA, and the SIMBAD database, operated at CDS, Strasbourg, France. The Center for Exoplanets and Habitable Worlds is supported by the Pennsylvania State University, the Eberly College of Science, and the Pennsylvania Space Grant Consortium.

REFERENCES

- Alcalá, J. M., Majidi, F. Z., Desidera, S., et al. 2020, *A&A*, 635, L1
- Alcalá, J. M., Manara, C. F., Natta, A., et al. 2017, *A&A*, 600, A20
- Alcalá, J. M., Natta, A., Manara, C. F., et al. 2014, *A&A*, 561, A2
- Allen, P. R., Luhman, K. L., Myers, P. C., et al. 2007, *ApJ*, 655, 1095
- Allers, K. N., Kessler-Silacci, J. E., Cieza, L. A., & Jaffe, D. T. 2006, *ApJ*, 644, 364
- André, P., Ward-Thompson, D., & Barsony, M. 1993, *ApJ*, 406, 122
- Appenzeller, I., Jankovics, I., & Krautter, J. 1983, *A&AS*, 53, 291
- Bailer-Jones, C. A. L., Rybizki, J., Fouesneau, M., Mantelet, G., & Andrae, R. 2018, *AJ*, 156, 58
- Baraffe, I., Chabrier, G., Allard, F., & Hauschildt, P. H. 1998, *A&A*, 337, 403
- Baraffe, I., Horneier, D., Allard, F., & Chabrier, G. 2015, *A&A*, 577, 42
- Bell, C. P. M., Mamajek, E. E., & Naylor, T. 2015, *MNRAS*, 454, 593
- Benedettini, M., Pezzuto, E., Schisano, E., et al. 2018, *A&A*, 619, A52
- Billar, B., Lacour, S., Juhász, A., et al. 2012, *ApJ*, 753, L38
- Blondel, P. F. C., & Tjin A Djie, H. R. E. 2006, *A&A*, 456, 1045
- Bustamante, I., Merín, B., Ribas, Á., et al. 2015, *A&A*, 578, A23
- Cannon, A. J., & Pickering, E. C. 1921, *The Henry Draper catalogue : 15h and 16h*, *Annals of Harvard College Observatory*, 96
- Cánovas, H., Cantero, C., Cieza, L., et al. 2019, *A&A*, 626, A80
- Chapman, N. L., Lai, S.-P., Mundy, L. G., et al. 2007, *ApJ*, 667, 288
- Choi, J., Dotter, A., Conroy, C., et al. 2016, *ApJ*, 823, 102
- Cieza, L., Padgett, D. L., Stapelfeldt, K. R., et al. 2007, *ApJ*, 667, 308
- Close, L. M., Follette, K. B., Males, J. R., et al. 2014, *ApJ*, 781, L30
- Comerón, F. 2008, in *Handbook of Star Forming Regions*, Vol. 2, *The Southern Sky*, ASP Monograph Series 5, ed. B. Reipurth (San Francisco, CA: ASP), 295
- Comerón, F. 2011, *A&A*, 531, A33
- Comerón, F., Fernández, M., Baraffe, I., Neuhäuser, R., & Kaas, A. A. 2003, *A&A*, 406, 1001
- Comerón, F., Spezzi, L., & López Martí, B. 2009, *A&A*, 500, 1045
- Comerón, F., Spezzi, L., López Martí, B., & merín, B. 2013, *A&A*, 554, A86
- Cook, N. J., Scholz, A., & Jayawardhana, R. 2017, *AJ*, 154, 256
- Cutri, R. M., Skrutskie, M. F., van Dyk, S., et al. 2012, *yCat*, 2281, 0
- Damiani, F., Prisinzano, L., Pillitteri, I., Micela, G., & Sciortino, S. 2019, *A&A*, 623, A112
- de Bruijne, J. H. J. 2012, *Ap&SS*, 341, 31
- de Zeeuw, P. T., Hoogerwerf, R., de Bruijne, J. H. J., Brown, A. G. A., & Blaauw, A. 1999, *AJ*, 117, 354
- Dotter, A. 2016, *ApJS*, 222, 8
- Dzib, S. A., Loinard, L., Ortiz-León, G. N., Rodríguez, L. F., & Galli, P. A. B. 2018, *ApJ*, 867, 151
- Espaillat, C., Ingleby, L., Hernandez, J., et al. 2012, *ApJ*, 747, 103
- Esplin, T. L., & Luhman, K. L. 2017, *AJ*, 154, 134
- Esplin, T. L., & Luhman, K. L. 2019, *AJ*, 158, 54
- Esplin, T. L., & Luhman, K. L. 2020, *AJ*, 159, 282
- Esplin, T. L., Luhman, K. L., & Mamajek, E. E. 2014, *ApJ*, 784, 126
- Esplin, T. L., Luhman, K. L., Miller, E. B., & Mamajek, E. E. 2018, *AJ*, 156, 75
- Evans, N. J. II, Allen, L. E., Blake, G. A., et al. 2003, *PASP*, 115, 965
- Fazio, G. G., Hora, J. L., Allen, L. E., et al. 2004, *ApJS*, 154, 10
- Feiden, G. A. 2016, *A&A*, 593, A99
- Frasca, A., Biazzo, K., Alcalá, J. M., et al. 2017, *A&A*, 602, A33
- Gaia Collaboration, Brown, A. G. A., Vallenari, A., Prusti, T., et al. 2018, *A&A*, 616, A1
- Gaia Collaboration, Prusti, T., de Bruijne, J. H. J., et al. 2016, *A&A*, 595, A1
- Galli, P. A. B., Bertout, C., Teixeira, R., & Ducourant, C. 2013, *A&A*, 558, A77
- Goldman, B., Röser, S., Schilbach, E., Moór, A. C., & Henning, T. 2018, *ApJ*, 868, 32
- Gontcharov, G. A. 2006, *AstL*, 32, 759
- Greene, T. P., Wilking, B. A., André, P., Young, E. T., & Lada, C. J. 1994, *ApJ*, 434, 614
- Herbig, G. H. 1977, *ApJ*, 214, 747
- Herczeg, G. J., & Hillenbrand, L. A. 2014, *ApJ*, 786, 97
- Hernández, J., Hartmann, L., Megeath, T., et al. 2007, *ApJ*, 662, 1067
- Heyer, M. H., & Graham, A. 1989, *PASP*, 101, 816
- Houk, N. 1982, *Michigan Catalogue of Two-dimensional Spectral Types for the HD Stars*. Vol. 2, (Ann Arbor: Univ. Mich.)
- Houk, N. 1982, *Michigan Catalogue of Two-dimensional Spectral Types for the HD Stars*. Vol. 3, (Ann Arbor: Univ. Mich.)
- Hughes, J., Hartigan, P., Krautter, J., & Kelemen, J. 1994, *AJ*, 108, 1071
- Indebetouw, R., Mathis, J. S., Babler, B. L., et al. 2005, *ApJ*, 619, 931
- Johnson D. R. H., & Soderblom D. R., 1987, *AJ*, 93, 864
- Juvela, M., & Montillaud, J. 2016, *A&A*, 585, A38
- Kenyon, S. J., & Bromley, B. C. 2005, *AJ*, 130, 269
- Köhler, R., Kunkel, M., Leinert, C., & Zinnecker, H. 2000, *A&A*, 356, 541
- Krautter, J., Wichmann, R., Schmitt, J. H. M. M., et al. 1997, *A&AS*, 123, 329
- Lada, C. J. 1987, in *IAU Symp. 115, Star Forming Regions*, ed. M. Peimbert & J. Jugaku (Dordrecht: Reidel), 1
- Lada, C. J., & Wilking, B. A. 1984, *ApJ*, 287, 610
- Lindgren, L. 2018, *Re-normalising the astrometric chi-square in Gaia DR2*, *GAIA-C3-TN-LU-LL-124-01*, http://www.rssd.esa.int/doc_fetch.php?id=3757412
- Lombardi, M., Lada, C. J., & Alves, J. 2008, *A&A*, 480, 785
- López Martí, B., Eisloffel, J., & Mundt, R. 2005, *A&A*, 440, 139
- Luhman, K. L. 2018, *AJ*, 156, 271
- Luhman, K. L., Allen, P. R., Espaillat, C., Hartmann, L., & Calvet, N. 2010, *ApJS*, 186, 111
- Luhman, K. L., & Esplin, T. L. 2020, *AJ*, 160, 44
- Luhman, K. L., Esplin, T. L., & Loutrel, N. P. 2016, *ApJ*, 827, 52
- Luhman, K. L., Herrmann, K. A., Mamajek, E. E., Esplin, T. L., & Pecaut, M. J. 2018, *AJ*, 156, 76
- Luhman, K. L., & Mamajek, E. E. 2012, *ApJ*, 758, 31
- Mamajek, E. E., Meyer, M. R., & Liebert, J. 2002, *AJ*, 124, 1670
- Manara, C. F., Prusti, T., Comerón, F., et al. 2018, *A&A*, 615, L1
- Manara, C. F., Testi, L., Natta, A., et al. 2014, *A&A*, 568, 18
- Manara, C. F., Testi, L., Rigliaco, E., et al. 2013, *A&A*, 551, 107
- Martín, E. L., Rebolo, R., & Magazzu, A. 1994, *ApJ*, 436, 262
- McMahon, R. G., Banerji, M., Gonzalez, E., et al. 2013, *The Messenger*, 154, 35
- Melton, E. 2020, *AJ*, 159, 200
- Merín, B., Brown, J. M., Oliveira, I., et al. 2010, *ApJ*, 718, 1200
- Merín, B., Jørgensen, J., Spezzi, L., et al. 2008, *ApJS*, 177, 551
- Mortier, A., Oliveira, I., & van Dishoeck, E. F. 2011, *MNRAS*, 418, 1194
- Mužić, K., Scholz, A., Geers, V. C., Jayawardhana, R. 2015, *ApJ*, 810, 159
- Mužić, K., Scholz, A., Geers, V. C., Jayawardhana, R., & López Martí, B. 2014, *ApJ*, 785, 159
- Nesterov, V. V., Kuzmin, A. V., Ashimbaeva, N. T., et al. 1995, *A&AS*, 110, 367
- Neuhäuser, R., et al. 2005, *A&A*, 435, L13
- Padgett, D. L., Cieza, L., Stapelfeldt, K. R., et al. 2006, *ApJ*, 645, 1283
- Pecaut, M. J., & Mamajek E. E. 2016, *MNRAS*, 461, 794
- Pecaut, M. J., Mamajek E. E., & Bubar E. J. 2012, *ApJ*, 746, 154
- Perryman, M. A. C., de Boer, K. S., Gilmore, G., et al. 2001, *A&A*, 369, 339
- Preibisch, T., & Mamajek, E. 2008, in *Handbook of Star Forming Regions*, Vol. 2, *The Southern Sky*, ASP Monograph Series 5, ed. B. Reipurth (San Francisco, CA: ASP), 235
- R Core Team, 2013, *R Foundation for Statistical Computing*, Vienna, Austria, <http://www.R-project.org>
- Rieke, G. H., Su, K. Y. L., Stansberry, J. A., et al. 2005, *ApJ*, 620, 1010
- Rieke, G. H., Young, E. T., Engelbracht, C. W., et al. 2004, *ApJS*, 154, 25

- Romero, G. A., Schreiber, M. R., Cieza, L. A., et al. 2012, *ApJ*, 749, 79
- Röser, S., Schilbach, E., Goldman, B., et al. 2018, *A&A*, 614, A18
- Schlaflý, E. F., Meisner, A. M., Stutz, A. M., et al. 2016, *ApJ*, 821, 78
- Schwartz, R. D. 1977, *ApJS*, 35, 161
- Scrucca L., Fop M., Murphy T. B., & Raftery A. E. 2016, *mclust* 5: clustering, classification and density estimation using Gaussian finite mixture models, *The R Journal*, 8, 205
- Skrutskie, M., Cutri, R. M., Stiening, R., et al. 2006, *AJ*, 131, 1163
- Spezzi, L., Vernazza, P., Merín, B., et al. 2011, *ApJ*, 730, 65
- Teixeira, P. S., Scholz, A., & Alves, J. 2020, *A&A*, in press
- Torres, C. A. O., Quast, G. R., da Silva, L., et al. 2006, *A&A*, 460, 695
- Waelkens, C., Waters, L. B. F. M., de Graauw, M. S., et al. 1996, *A&A*, 315, L245
- Wahhaj, Z., Cieza, L., Koerner, D. W., et al. 2010, *ApJ*, 724, 835
- Werner, M. W., Roellig, T. L., Low, F. J., et al. 2004, *ApJS*, 154, 1
- Wichmann, R., Covino, E., & Alcalá, J. M. 1999, *MNRAS*, 307, 909
- Wilkinson, S., Merín, B., & Riviere-Marichalar, P. 2018, *A&A*, 618, A12
- Wright, E. L., Eisenhardt, P. R., Mainzer, A. K., et al. 2010, *AJ*, 140, 1868
- Zucker, C., Speagle, J. S., Schlafly, E. F., et al. 2020, *A&A*, 633, A51

TABLE 1
CANDIDATE MEMBERS OF LUPUS AT $l = 335\text{--}345^\circ$ AND $b = 5\text{--}19^\circ$ THAT HAVE
GAIA KINEMATICS

Column Label	Description
Gaia	Gaia DR2 source name
2MASS	2MASS Point Source Catalog source name
WISEA	AllWISE Source Catalog source name
Name	Other source name
RAdeg	Right Ascension from Gaia DR2 (J2000)
DEdeg	Declination from Gaia DR2 (J2000)
SpType	Spectral type
r.SpType	Spectral type reference ^a
pmRA	Proper motion in right ascension from Gaia DR2
e.pmRA	Error in pmRA
pmDec	Proper motion in declination from Gaia DR2
e.pmDec	Error in pmDec
plx	Parallax from Gaia DR2
e.plx	Error in plx
RVel	Radial velocity
e.RVel	Error in RVel
r.RVel	Radial velocity reference ^b
U	U component of space velocity
e.U	Error in U
V	V component of space velocity
e.V	Error in V
W	W component of space velocity
e.W	Error in W
Gmag	G magnitude from Gaia DR2
e.Gmag	Error in Gmag
GBPmag	G_{BP} magnitude from Gaia DR2
e.GBPmag	Error in GBPmag
GRPmag	G_{RP} magnitude from Gaia DR2
e.GRPmag	Error in GRPmag
RUWE	renormalized unit weight error from Lindegren (2018)
Jmag	J magnitude
e.Jmag	Error in Jmag
Hmag	H magnitude
e.Hmag	Error in Hmag
Ksmag	K_s magnitude
e.Ksmag	Error in Ksmag
JHKref	JHK_s reference ^c
W1mag	WISE W1 magnitude
e.W1mag	Error in W1mag
f.W1mag	Flag on W1mag ^d
W2mag	WISE W2 magnitude
e.W2mag	Error in W2mag
f.W2mag	Flag on W2mag ^d
W3mag	WISE W3 magnitude
e.W3mag	Error in W3mag
f.W3mag	Flag on W3mag ^d
W4mag	WISE W4 magnitude
e.W4mag	Error in W4mag
f.W4mag	Flag on W4mag ^d
ExcW2	Excess present in W2?
ExcW3	Excess present in W3?
ExcW4	Excess present in W4?
Exc4.5	Excess present in $[4.5]?$
Exc8.0	Excess present in $[8.0]?$
Exc24	Excess present in $[24]?$
DiskType	Disk Type
OnCloud	Near Lupus clouds 1–4? ^e

TABLE 1 — *Continued*

Column Label	Description
--------------	-------------

NOTE. — This table is available in its entirety in a machine-readable form.

^a (1) Krautter et al. (1997); (2) Torres et al. (2006); (3) Appenzeller et al. (1983); (4) Heyer & Graham (1989); (5) Hughes et al. (1994); (6) Köhler et al. (2000); (7) Herczeg & Hillenbrand (2014); (8) Alcalá et al. (2017); (9) Alcalá et al. (2014); (10) Herbig (1977); (11) Alcalá et al. (2020); (12) Martín et al. (1994); (13) Houk (1978); (14) Pecaut & Mamajek (2016); (15) Mortier et al. (2011); (16) Romero et al. (2012); (17) Cannon & Pickering (1921); (18) Houk (1982); (19) Comerón et al. (2013); (20) Mužić et al. (2014); (21) Allen et al. (2007); (22) Comerón et al. (2003); (23) Manara et al. (2013); (24) Mužić et al. (2015); (25) Blondel & Tjin A Djie (2006); (26) Manara et al. (2014); (27) Mamajek et al. (2002); (28) Nesterov et al. (1995).

^b (1) Gaia DR2; (2) Frasca et al. (2017); (3) Galli et al. (2013); (4) Torres et al. (2006); (5) Alcalá et al. (2020); (6) Gontcharov (2006); (7) Wichmann et al. (1999).

^c 2 = 2MASS Point Source Catalog; 6 = 2MASS 6X Point Source Working Database (Cutri et al. 2012); a = Alcalá et al. (2014); v = sixth data release of the Visible and Infrared Survey Telescope for Astronomy (VISTA) Hemisphere Survey (VHS, McMahon et al. 2013).

^d nodet = non-detection; sat = saturated; bl = photometry may be affected by blending with a nearby star; bin = includes an unresolved binary companion; unres = too close to a brighter star to be detected; false = detection from WISE catalog appears false or unreliable based on visual inspection; err = W2 magnitudes brighter than ~ 6 are erroneous.

^e Indicates whether the star is located within one of the circular and elliptical fields encompassing clouds 1–4 in Figure 1.

TABLE 2
ON-CLOUD CANDIDATE MEMBERS OF LUPUS THAT LACK GAIA KINEMATICS

Column Label	Description
Gaia	Gaia DR2 source name
2MASS	2MASS Point Source Catalog source name
WISEA	AllWISE Source Catalog source name
Name	Other source name
RAdeg	Right Ascension (J2000) ^a
DEdeg	Declination (J2000) ^a
SpType	Spectral type
r_SpType	Spectral type reference ^b
Gmag	G magnitude from Gaia DR2
e_Gmag	Error in Gmag
GBPmag	G_{BP} magnitude from Gaia DR2
e_GBPmag	Error in GBPmag
GRPmag	G_{RP} magnitude from Gaia DR2
e_GRPmag	Error in GRPmag
RUWE	renormalized unit weight error from Lindegren (2018)
Jmag	J magnitude
e_Jmag	Error in Jmag
Hmag	H magnitude
e_Hmag	Error in Hmag
Ksmag	K_s magnitude
e_Ksmag	Error in Ksmag
JHKref	JHK_s reference ^c
W1mag	WISE W1 magnitude
e_W1mag	Error in W1mag
f_W1mag	Flag on W1mag ^d
W2mag	WISE W2 magnitude
e_W2mag	Error in W2mag
f_W2mag	Flag on W2mag ^d
W3mag	WISE W3 magnitude
e_W3mag	Error in W3mag
f_W3mag	Flag on W3mag ^d
W4mag	WISE W4 magnitude
e_W4mag	Error in W4mag
f_W4mag	Flag on W4mag ^d
ExcW2	Excess present in W2?
ExcW3	Excess present in W3?
ExcW4	Excess present in W4?
Exc4.5	Excess present in [4.5]?
Exc8.0	Excess present in [8.0]?
Exc24	Excess present in [24]?
DiskType	Disk Type

NOTE. — This table is available in its entirety in a machine-readable form.

^a Right ascension and declination are from Gaia DR2, the 2MASS Point Source Catalog, and the AllWISE Source Catalog in order of preference.

^b (1) Heyer & Graham (1989); (2) Hughes et al. (1994); (3) Alcalá et al. (2014); (4) Mortier et al. (2011); (5) Alcalá et al. (2017); (6) Krautter et al. (1997); (7) Romero et al. (2012); (8) Comerón et al. (2013).

^c 2 = 2MASS Point Source Catalog; 6 = 2MASS 6X Point Source Working Database (Cutri et al. 2012); v = sixth data release of VISTA VHS.

^d nodet = non-detection; bl = photometry may be affected by blending with a nearby star; ext = photometry is contaminated by extended emission; bin = includes an unresolved binary companion; unres = too close to a brighter star to be detected; false = detection from WISE catalog appears false or unreliable based on visual inspection; err = W2 magnitudes brighter than ~ 6 are erroneous.

TABLE 3
 MEDIAN AND STANDARD DEVIATIONS OF SPACE VELOCITIES OF ON-CLOUD
 LUPUS CANDIDATES

Cloud	U	V (km s ⁻¹)	W	σ_U	σ_V (km s ⁻¹)	σ_W	N_*
1	-5.0	-18.3	-5.7	3.4	1.6	1.3	12
2	-5.3	-17.6	-7.1	2.2	0.9	0.4	5
3	-2.9	-17.9	-7.6	3.7	1.6	1.0	44
4	-4.1	-18.1	-7.3	1.8	0.9	0.8	8
1-4	-3.5	-18.0	-7.2	3.4	1.5	1.2	69

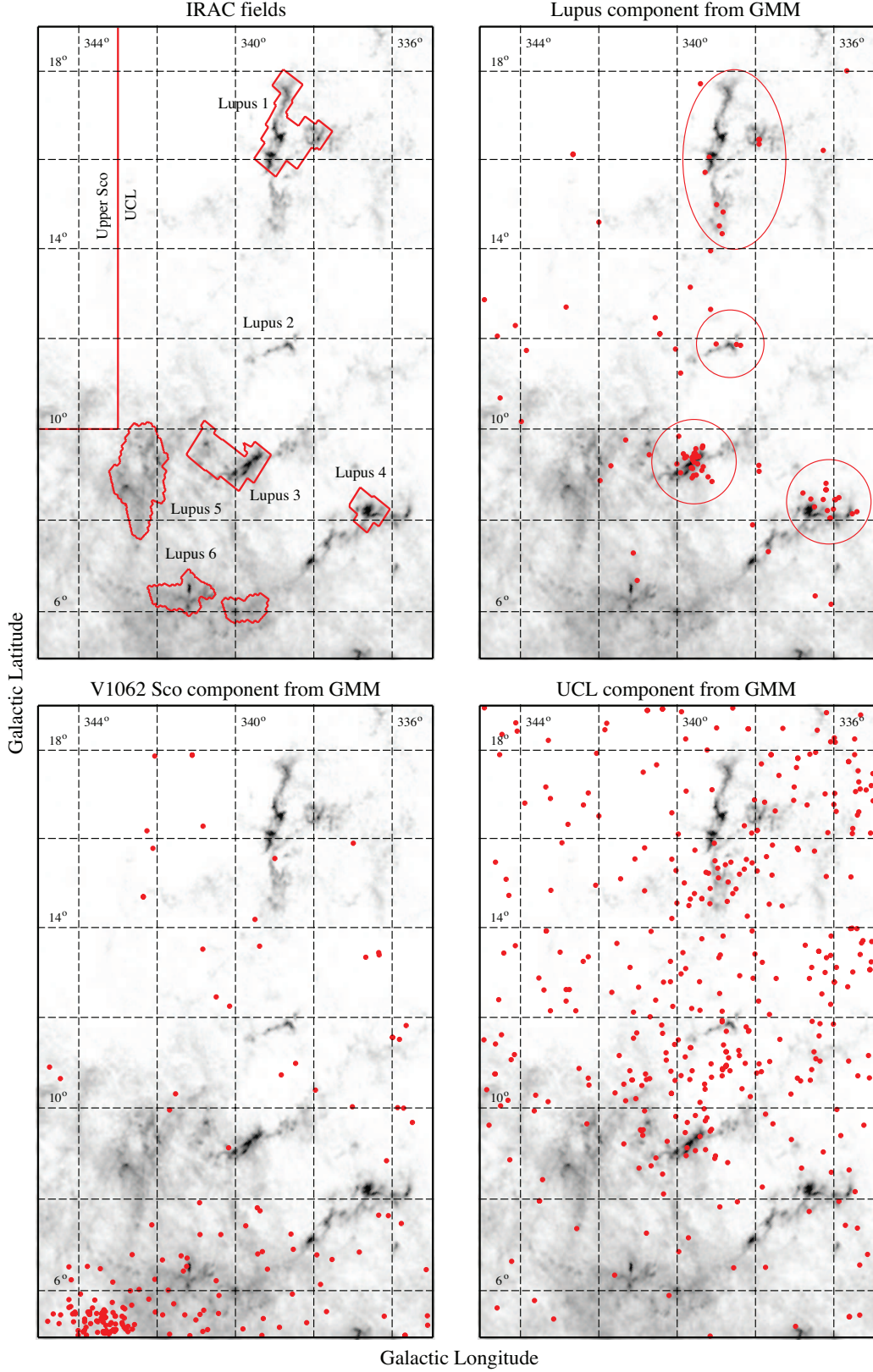


FIG. 1.— Maps of the fields toward the Lupus clouds that were imaged by IRAC during the cryogenic phase of Spitzer and the three kinematic populations of candidate young stars identified with a GMM in the middle panel of Figure 2. Extinction ranging from $A_K = 0.2$ – 2.5 is displayed with the gray scale (Juvela & Montillaud 2016). The members of the Lupus population that are within the circular and elliptical fields encompassing clouds 1–4 are used to define the kinematics of stars associated with those clouds (bottom panel of Figure 2). The map of the IRAC fields includes the boundary between Upper Sco and UCL from de Zeeuw et al. (1999).

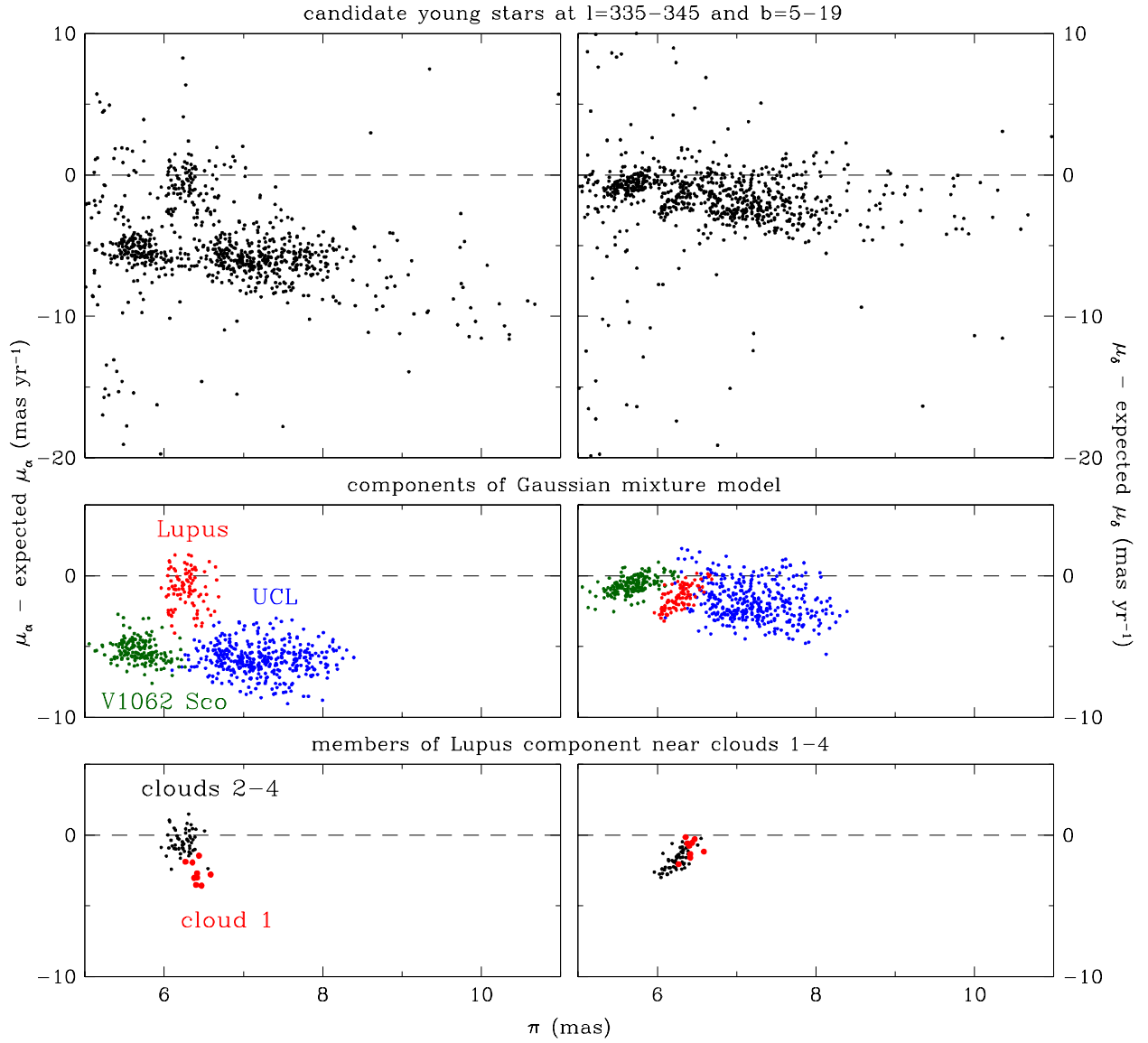


FIG. 2.— Proper motion offsets versus parallax for candidate young low-mass stars ($G_{BP} - G_{RP}=1.4-3.4$, $\sim 0.15-1 M_\odot$) within the boundaries of the maps in Figure 1 (top). The offsets are computed relative to the proper motions expected for the positions and parallaxes assuming the median space velocity of Upper Sco members (Section 2.1). A GMM has been used to estimate probabilities of membership in three clustered components and a more widely scattered field component. The stars are plotted with colors corresponding to the components to which they most likely belong, excluding probable members of the field component (middle). Those three components are plotted on maps in Figure 1 and contain members of the V1062 Sco, UCL, and the Lupus clouds. The members of the Lupus component within the circular and elliptical fields from Figure 1 are plotted to further refine the kinematics of stars associated with the Lupus clouds (bottom).

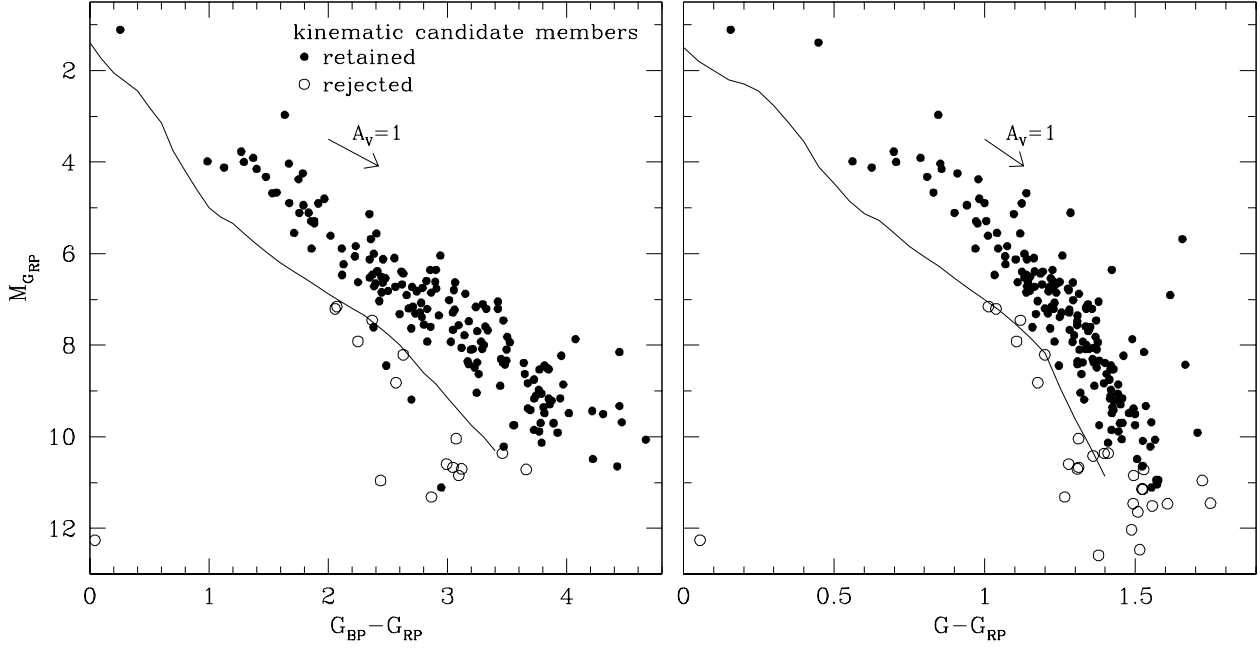


FIG. 3.— $M_{G_{RP}}$ versus $G_{BP} - G_{RP}$ and $G - G_{RP}$ for candidate members of Lupus selected via their kinematics from Gaia DR2, which consist of stars that have positions within the boundaries of the maps in Figure 1, $\pi/\sigma \geq 10$, and parallaxes and proper motion offsets overlapping with those of the stars in the bottom panel of Figure 2. Each diagram includes a fit to the single-star sequence for the Tuc-Hor association (45 Myr, Bell et al. 2015) (solid line). Stars that appear above the Tuc-Hor sequence in either diagram or exhibit mid-IR excess emission from a circumstellar disk are retained as candidate members of Lupus (filled circles) while the remaining stars are rejected (open circles). The reddening vectors are based on the extinction curve from Schlafly et al. (2016).

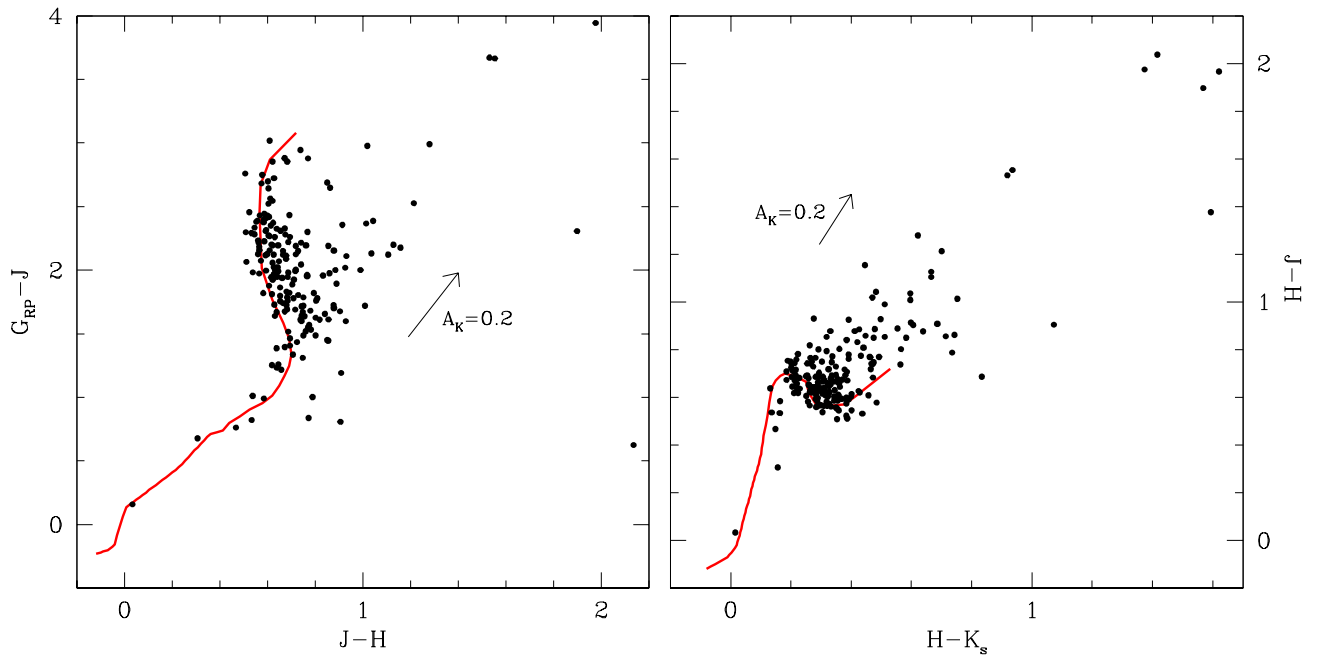


FIG. 4.— $G_{\text{RP}} - J$ versus $J - H$ and $J - H$ versus $H - K_s$ for candidate members of Lupus from Tables 1 and 2 (filled circles). The intrinsic colors of young stars from B0-M9 are indicated (red solid lines, Luhman & Esplin 2020).

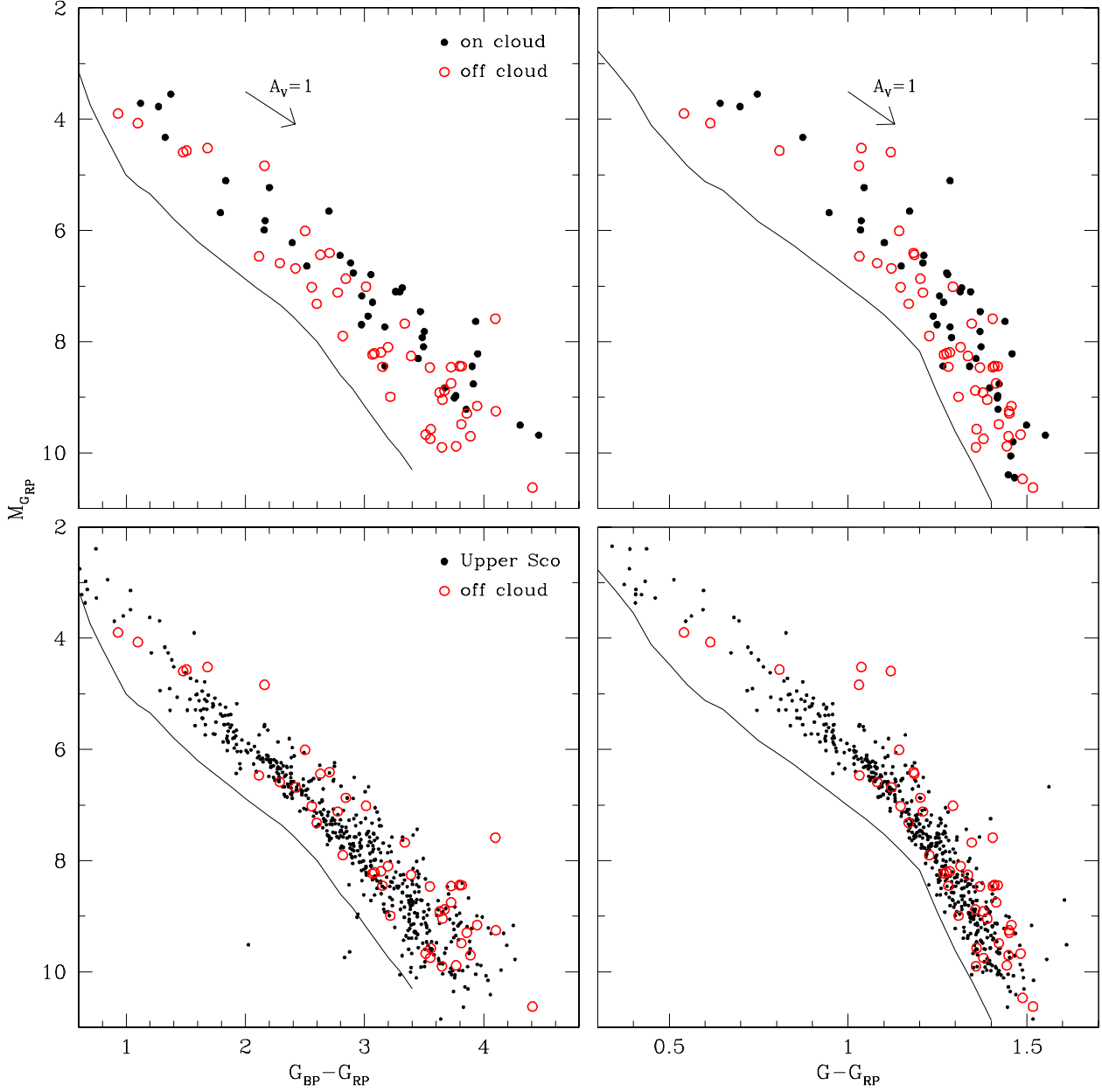


FIG. 5.— Extinction-corrected $M_{G_{RP}}$ versus $G_{BP} - G_{RP}$ and $G - G_{RP}$ for the candidate members of Lupus from Table 1 that have precise parallaxes ($\pi/\sigma \geq 20$) and low extinctions ($A_K < 0.2$) and do not have full disks (top). Candidates within the circular and elliptical fields in Figure 1 are plotted with filled circles and candidates outside of those fields are plotted with open circles. The off-cloud candidates are shown with members of Upper Sco that have $\pi/\sigma \geq 20$ and $A_K < 0.1$ and that lack disks (bottom). Each diagram includes a fit to the single-star sequence for the Tuc-Hor association (45 Myr, Bell et al. 2015) (solid line).

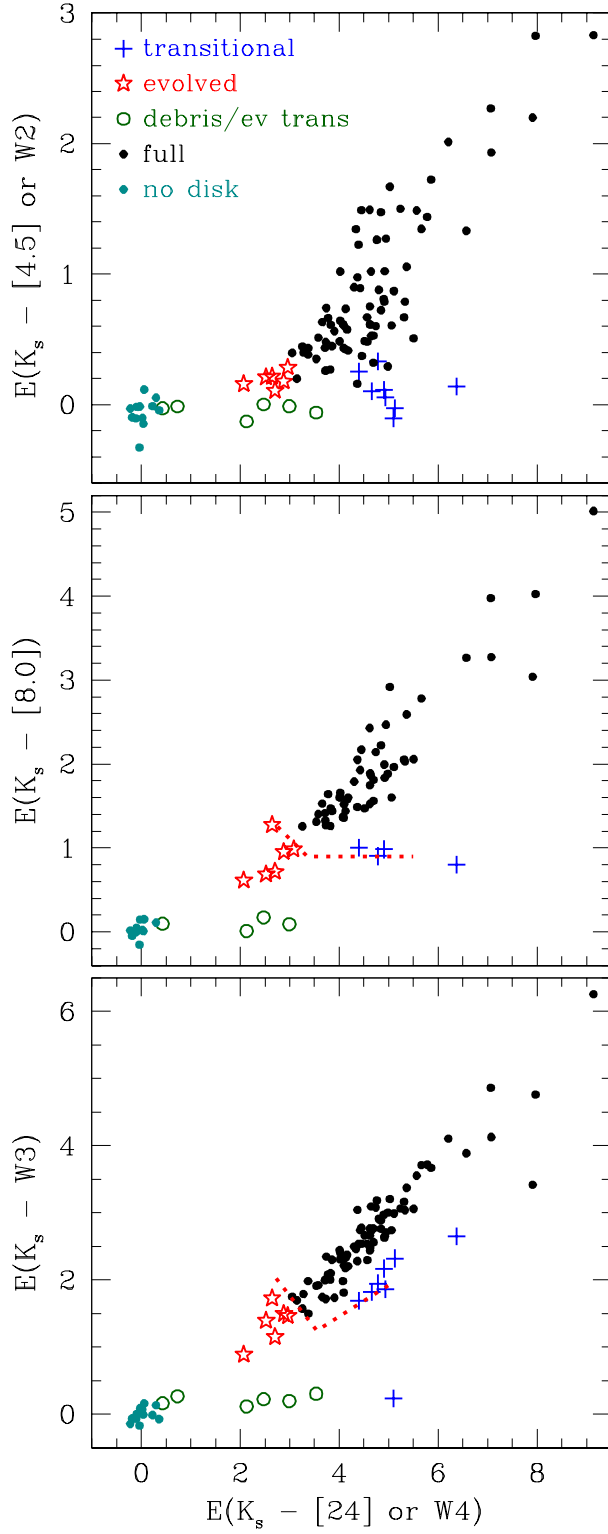


FIG. 6.— Extinction-corrected IR color excesses for candidate members of Lupus from Tables 1 and 2. Data at $[4.5]$ and $[24]$ are shown when available. Otherwise, measurements at similar wavelengths from WISE are used (W2 and W4). The bottom two diagrams include boundaries that are used to distinguish full disks from disks in more advanced stages of evolution (dotted lines).

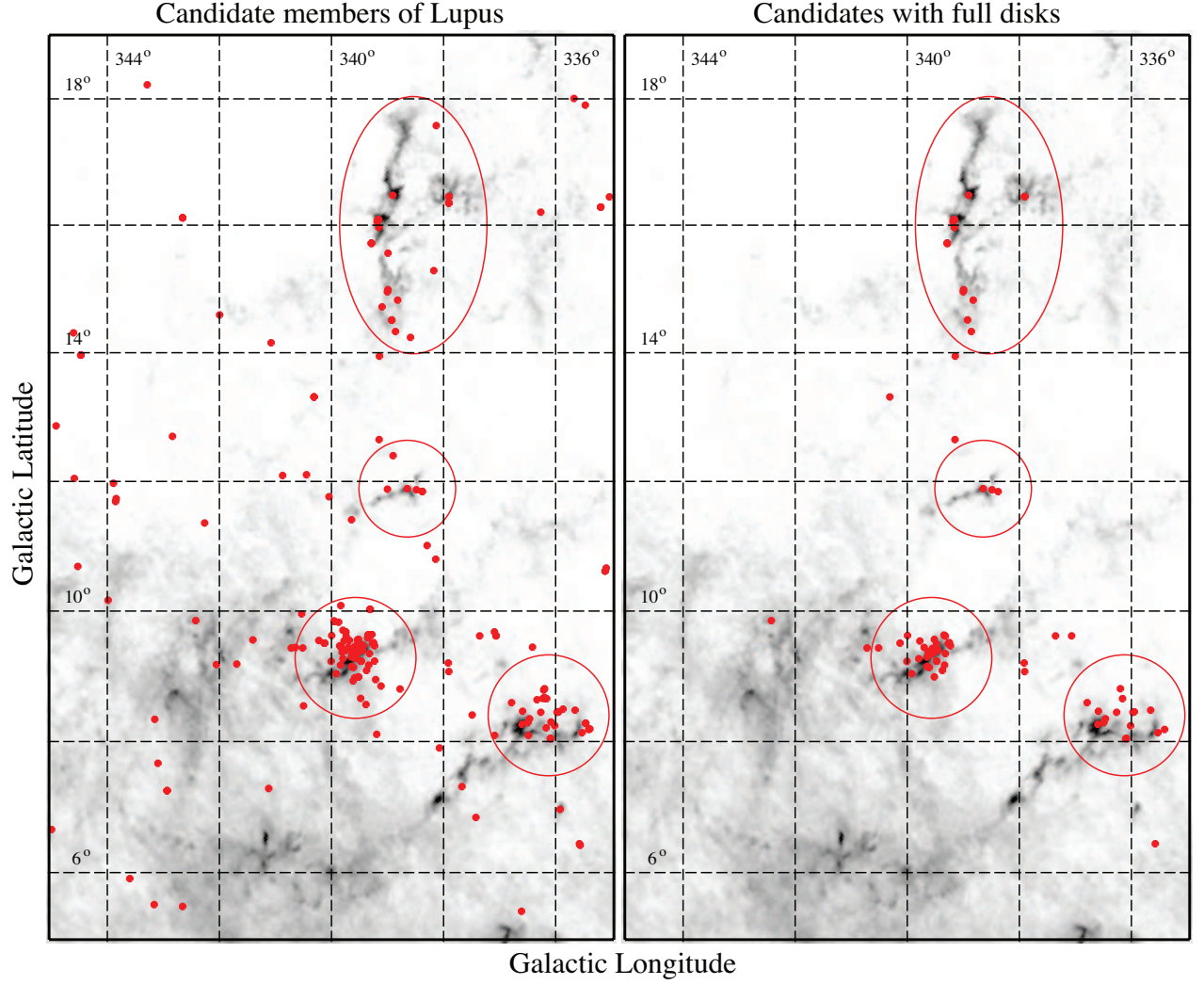


FIG. 7.— Map of the candidate members of Lupus from Tables 1 and 2 and the subset of those candidates with full disks. Extinction ranging from $A_K = 0.2$ – 2.5 is displayed with the gray scale (Juvela & Montillaud 2016).

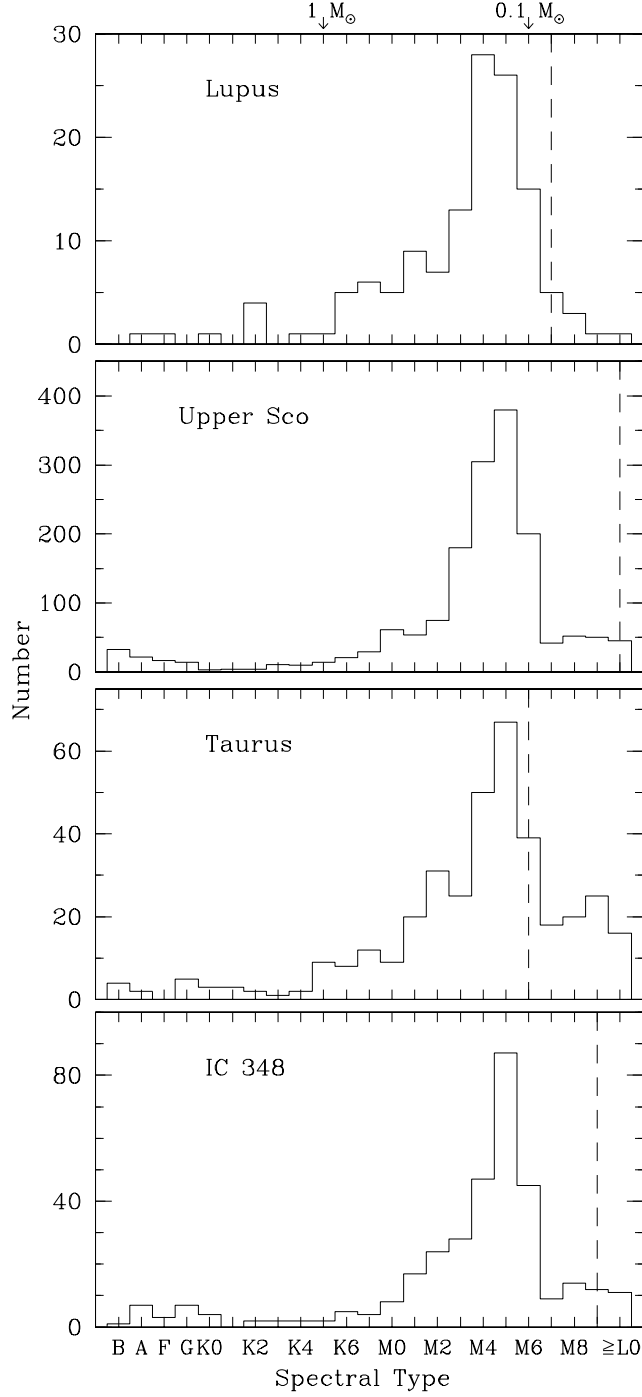


FIG. 8.— Distribution of spectral types for candidate members of Lupus from Tables 1 and 2 that have $A_K < 0.2$ and are within the circular and elliptical fields in Figure 1 and distributions for members of Upper Sco (Luhman & Esplin 2020), Taurus ($A_J < 1$, Esplin & Luhman 2019), and IC 348 ($A_J < 1.5$, Luhman et al. 2016). The dashed lines indicate the completeness limits of these samples and the arrows mark the spectral types that correspond to masses of 0.1 and $1 M_{\odot}$ for ages of a few Myr according to evolutionary models (e.g., Baraffe et al. 1998, 2015).